https://doi.org/10.5194/essd-2020-85
Preprint. Discussion started: 17 July 2020

A long-term (2005-2016) dataset of integrated land-atmosphere interaction observations on the Tibetan Plateau

Yaoming Ma[1,3,4], Zeyong Hu[2,3], Zhipeng Xie[1,2], Weiqiang Ma[1,3], Binbin Wang[1], Xuelong Chen[1], Maoshan Li[5], Lei Zhong[6,7], Fanglin Sun[2], Lianglei Gu[2], Cunbo Han[1], Lang Zhang[1], Xin Liu[1], Zhangwei Ding[1], Genhou Sun[8], Shujin Wang[2], Yongjie Wang[1], Zhongyan Wang[1]

[1] Key Laboratory of Tibetan Environment Changes and Land Surface Processes, Institute of Tibetan Plateau Research, Chinese Academy of Sciences, Beijing, 100101, China.
[2] Key Laboratory of Land Surface Process and Climate Change in Cold and Arid Regions, Northwest Institute of Eco-Environment and Resources, Chinese Academy of Sciences, Lanzhou, 730000, China.
[3] CAS Center for Excellence in Tibetan Plateau Earth Sciences, Beijing, 100101, China.
[4] University of Chinese Academy of Sciences, 100049, Beijing, China.
[5] School of Atmospheric Sciences, Chengdu University of Information Technology, Chengdu, 610025, China.
[6] School of Earth and Space Sciences, University of Science and Technology of China, Hefei, 230026, China.
[7] CAS Center for Excellence in Comparative Planetology, USTC, Hefei, 230026, China.
[8] School of Atmospheric Sciences, Sun Yat-sen University, Guangzhou, 510275, China.

Correspondence to: Yaoming Ma (ymma@itpcas.ac.cn), Zhipeng Xie (zp_xie@itpcas.ac.cn) and Binbin Wang (wangbinbin@itpcas.ac.cn)

Abstract. The Tibetan Plateau (TP) plays a critical role in influencing regional and global climate, via both thermal and dynamical mechanisms. Meanwhile, as the largest high-elevation part of the cryosphere outside the polar regions, with vast areas of mountain glaciers, permafrost and seasonally frozen ground, the TP is characterized as an area sensitive to global climate change. However, meteorological stations are sparsely and biased distributed over the TP, owing to the harsh environmental conditions, high elevations, complex topography, and heterogeneous surfaces. Moreover, due to the weak representation of the stations, atmospheric conditions and the local land-atmosphere coupled system over the TP as well as its effects on surrounding regions are poorly quantified. This paper presents a long-term (2005-2016) dataset of hourly land-atmosphere interaction observations from an integrated high-elevation, cold region observation network, which is composed of six field observation and research platforms on the TP. In-situ observations, at the hourly resolution, consisting of measurements of micrometeorology, surface radiation, eddy covariance (EC), and soil temperature and soil water content profiles. Meteorological data were monitored by an automatic weather station (AWS) or a planetary boundary layer (PBL) observation system composed of multiple meteorological element instruments. Multilayer soil hydrothermal data were recorded to capture vertical variations in soil temperature and water content and to study the freeze-thaw process. In addition, to capture the high-frequency vertical exchanges of energy, momentum, water vapor and carbon dioxide within the atmospheric boundary layer, an EC system consisting of an ultrasonic anemometer and an infrared gas analyzer was installed at each station. The release of these continuous and long-term datasets with hourly time resolution represents a leap forward in scientific data sharing across the TP, and it has been partially used in the past to assist in understanding key land surface processes. This dataset is described here comprehensively for facilitating a broader multidisciplinary community by enabling the evaluation and development of existing or new remote sensing algorithms as well as geophysical models for climate research and forecasting. The whole datasets are freely available at Science Data Bank (http://www.dx.doi.org/10.11922/sciencedb.00103, Ma et al., 2020) and, additionally at the National Tibetan Plateau Data Center (https://data.tpdc.ac.cn/en/data/b9ab35b2-81fb-4330-925f-4d9860ac47c3/).

1 Introduction

Referred to as the "Third Pole of the World" (Qiu,2008) , the TP, which is the world's highest and largest plateau and has highly complex terrain, plays an essential role in controlling regional and global climate through its thermal and mechanical mechanisms (Manabe and Broccoli, 1990;Yanai et al., 1992;Duan and Wu, 2005;Ma et al., 2006; Liu et al., 2007; Ma et al., 2008). The TP is also the most extensive high-elevation part of the cryosphere outside the polar regions, with vast areas of mountain glaciers, snow, permafrost and seasonally frozen ground distributed across the TP (Zhou and Guo, 1982; Kang et al., 2010; Cheng and Jin, 2013). The TP acts as the "Water Tower of Asia" (Immerzeel et al., 2010) and is highly sensitive to climate change (Pepin and Lundquist, 2008; Kang et al., 2010; Chen et al., 2015). In addition, under the influences of latent heat release (Wu et al., 2016) and the interactions between the Asian monsoon and mid-latitude westerlies (Yao et al., 2012), the TP exerts a major control on atmospheric circulation at the local and continental scale (Ding, 1992; Ye and Wu, 1998; Li et al., 2018).

The TP is the driving force for both regional environmental change, and amplifies environmental changes on a global scale (Pan et al., 1996; Kang et al., 2010). Land-atmosphere interactions over the TP play a crucial role in controlling the pattern and evolution of hemispheric atmospheric circulation and climate (Yang et al., 2004; Duan and Wu, 2005; Xiao and Duan, 2016; Li et al., 2018). Previous studies have revealed that accurate simulation of water and heat flux exchanges between the land surface and the atmosphere is a pivotal step towards improving the predictability and the projection accuracy of the climate system (Sellers et al., 1997; Pitman, 2003); this can be achieved through a comprehensive and accurate understanding of the land-atmosphere interactions based on in-situ observations (Yang et al., 2009). However, compared with other terrestrial regions of the world, observational data are scarce over the TP, owing to its vast geographic area with steep terrain, varied landforms, complex and diverse climates, harsh environmental conditions, and sparse and biased spatial distribution of observation stations relative to the high degree of landscape heterogeneity. In addition, there are high uncertainties in the satellite-retrieved land and atmospheric environmental variables of the TP, impairing the establishment of continuous, long-term regional-scale observations in remote areas. These problems have limited our understanding of the mechanisms underlying complex interactions between the different earth spheres with heterogeneous land surface conditions, thereby hindering the development of parameterization schemes in some critical physical processes of the land surface and atmospheric boundary layer. These issues lead to associated uncertainties in estimating the past, present, and future climate change and its impacts. Therefore, improving the atmospheric observation capability on the TP and its surrounding areas, and obtaining accurate atmospheric physical parameters for the near-surface and boundary layers over the TP could make a significant contribution to the scientific understanding of the weather, climate and environmental changes, as well as their impacts, from regional scale (TP) to global scale.

To mitigate the scarcity of observational data and to improve our understanding of the coupled local land-atmosphere system and its effects, a series of atmospheric field experiments have been carried out over the TP since the 1970s. For example, the first Qinghai-Xizang Plateau Meteorology Experiment (QXPMEX) (Tao et al., 1986), the Global Energy and Water Cycle Experiment (GEWEX) Asian Monsoon Experiment (GAME)/Tibet intensive observation (Wang, 1999), the Coordinated Enhanced Observing Period (CEOP) Asia–Australia Monsoon Project on the Tibetan Plateau (CAMP/ Tibet) (Ma et al., 2006), and so on. Several field observational stations have been established based on the comprehensive meteorological experiments carried out over the past few decades. After decades of effort, with an optimized scientific design and layout, the synthesis level of atmospheric observation has been greatly enhanced and improved in terms of the observation infrastructure and technology used, and meteorological elements observed. As a result, the limitations of the layout and function of the observation network over the TP have been mitigated to some extent. With the construction of the Tibetan Observation and Research Platform (TORP, Ma et al., 2008) and the implementation of long-term multi-site collaborative field experiments, a large volume of land surface processes and PBL observations have been collected, playing a crucial role in many disciplines: these include land-atmosphere interactions (Wang et al., 2017; Xie et al., 2018; Zhong et al., 2019), the characteristics of the PBL and troposphere (Sun et al., 2006; Li et al., 2012; Ma et al., 2015; Chen et al., 2016), and the development of land surface parameterization schemes (Yang et al., 2003; Chen et al., 2013).

The aforementioned field experiments and multi-site collaborative observations have yielded significant progress in advancing our understanding of the land-atmosphere interactions. However, integrated observations from field stations over the TP are still not open for sharing and only very limited data are available. Some in-situ observations can be obtained only through cooperation; others are restricted (e.g., only limited variables during a specified period are provided). Although some meteorological observations can be requested from the National Tibetan Plateau Data Center (TPDC) in recent years (http://www.tpdc.ac.cn), only the daily mean values, which lack consistent and standard data processing methods, are provided. Thus, the temporal resolution of these observations is too coarse for the land and climate modeling community, for which at least hourly measurements of meteorological variables are required to run and to evaluate detailed physical models. To overcome the above issues, a continuous and long-term integrated land-atmosphere interaction observational dataset with high temporal resolution is now provided (Ma et al., 2020). The underlying observation network is composed of meteorological gradient observations, surface radiation measurements, EC measurements and soil hydrothermal observations from six stations over the TP. This dataset has been released in a unified format that can be easily accessed and used by many communities, to facilitate consistency and continuity in scientific understanding of the interactions among the multi-sphere coupled systems over the TP. We expect this dataset will be widely used in studying the environment of the "Third Pole", especially by the atmosphere, hydrology, ecology and cryosphere communities; it will also promote the sharing, opening and value-added exploitation of the in-situ land-atmosphere interaction observations over the TP.

In this paper, we introduce and provide access to the long-term hourly dataset of the integrated land-atmosphere interaction observations over the TP. The integrated land-atmosphere interaction observation network is first described in Section 2. Section 3 deals specifically with a description of the meteorological, solar radiation, EC and soil hydrothermal data, and presents an overview of the observation infrastructure, highlighting differences and similarities between the stations in terms of the observation items, and their variations at diurnal, daily and monthly scales. The availability of this dataset is documented in Section 4 and a final summary is presented in Section 5.

2 Site descriptions

The integrated land-atmosphere interaction observation network in this study consists of six field stations (Figure 1), comprising the Muztagh Ata Westerly Observation and Research Station, Chinese Academy of Sciences (MAWORS, CAS); the Ngari Desert Observation and Research Station, CAS (NADORS) located in the northwestern TP; the BJ site of Nagqu Station of Plateau Climate and Environment, CAS (NPCE-BJ, hereinafter abbreviated to BJ) in the central TP; the Nam Co Monitoring and Research Station for Multisphere Interactions, CAS (NAMORS) on the banks of Lake Nam Co, as well as the Qomolangma Atmospheric and Environmental Observation and Research Station, CAS (QOMS) in the north region of Mt. Everest; and the Southeast Tibet Observation and Research Station for the Alpine Environment, CAS (SETORS) closed to the forested southeastern TP. This high-cold region observation network is an essential component of the meteorological observation platform over the TP, and provides valuable land surface processes observations, in areas currently lacking in-situ observations. Five stations (MAWORS, NADORS, NAMORS, QOMS, SETORS) were established and are maintained by the Institute of Tibetan Plateau Research (ITP), CAS while the BJ site is maintained by the Northwest Institute of Eco-Environment and Resources (NIEER), CAS. The coordinates and elevations of the stations are listed in Table 1, with elevations ranging from 3327 to 4730 m, and landscapes covering the dominant types of land cover on the TP (including alpine steppe with sparse vegetation, densely vegetated alpine meadow and alpine desert). The soil texture is dominated by sand and gravel in stations with sparsely covered vegetation (e.g., NADORS and QOMS) and silt and loam/clay in stations with dense vegetation (e.g., SETORS and BJ).

These stations serve as key locations for field observations and experiments: in particular, for monitoring the interactions between geological processes and climate; for collecting first-hand, high-resolution records of modern environmental variations; and for monitoring land surface processes and atmospheric processes. The observation system at each station primarily includes the following four categories of measurements: meteorological variables either from the PBL tower or the AWS, solar radiation components, eddy covariance fluxes and soil temperature and soil moisture. The meteorological instruments consist of up to 5 levels of wind speed and direction, air temperature and relative humidity instruments, in addition to surface air pressure and precipitation. The surface radiation components include the incoming and outgoing shortwave and longwave radiations. The open-path EC turbulent flux measurement system is used to sample the high frequency vertical turbulent fluxes of the sensible heat flux, latent heat flux and carbon dioxide flux. Vertical profiles of soil temperature and soil moisture content are monitored by multilayer temperature probes and water content reflectometers (5 or 6 layers). A list of the detailed information on observation items can be found in Table 2, which summarizes all the instruments used, including the layer configuration of the PBL tower and soil profile monitoring system, details of sensor models and manufacturers, and other information about the equipment used.

3 Integrated land-atmosphere interaction observations

3.1 Meteorological observations

To fully characterize the meteorological conditions and their vertical distributions in the surface layer, instruments were installed at several heights on a multi-layer PBL tower (QOMS, NAMORS, SETORS and BJ). For stations without a PBL tower, meteorological conditions are provided by a one-layer AWS at MAWORS and two-layer AWS at NADORS. There are significant differences in the layer configuration at each station. For example, five layers of wind speed and wind direction anemometers, air temperature and humidity probes were installed at QOMS and NAMORS; four layers of sensors were installed at SETORS; for BJ, three layers of wind and two layers of air temperature and relative humidity probes were available during 2006-2014, while four levels of these measurements were provided during 2015-2016 (see Table 2 for details). Besides, a surface pressure barometer and precipitation gauge are available at all the stations except in MAWORS, where precipitation is not measured. The meteorological elements of each station are detailed in the following sections, starting with the observation infrastructure, and followed by variations of the climatological average meteorological variables (except for wind direction and precipitation) at the lowest level of each station. We should note that the term "climatological" here does not strictly follow the definition recommended by the World Meteorological Organization (WMO), for which averages are based on 30 years of data. Here, "climatological" refers to the period for which variables are available at each station. At BJ, the climatological averages of wind speed, air temperature, relative humidity and pressure were calculated from 2006 to 2014.

3.1.1 Wind speed and wind direction

Wind speed and wind direction were monitored using non-heated anemometers at NADORS, MAWORS, NAMORS, QOMS, and SETORS, while they are heated ultrasonic anemometers at BJ. At NADORS and MAWORS, the horizontal wind variations were monitored at heights of 1.5 and 2 m above the ground, respectively. At the NAMORS and QOMS, wind sensors were measured at heights of 1.5, 2, 4, 10 and 20 m, while wind direction was only available at 1.5, 10 and 20 m. At SETORS, wind speed and wind direction were measured at four levels (1.3, 4.94, 9.95 and 18 m). At BJ, three layers of wind speed (at heights of 0.91, 5.02 and 10.36 m) and one-layer wind direction (at a height of 10.36 m) were available from 2006 to 2014 while wind measurements were available at four levels (1.5, 3, 6, and 12 m) during 2015-2016.

The climatological averaged wind speeds at diurnal, daily and monthly scales are shown in Figure 2 (a-c). Clear interdiurnal variations were observed, characterizing with a maximum in the afternoon and a constant wind speed in the early morning and throughout the night. At the diurnal scale, wind speed at SETORS showed the lowest diurnal variation throughout the year, while that at BJ showed the largest variations (the multi-year average here reached 8.13 m/s in the afternoon in January). At BJ, MAWORS, NADORS and NAMORS, the variations in wind speed in winter (December, January and February) were larger than those in the other seasons, while the greatest variability was observed in spring and early summer at QOMS. Significant differences exist in the climatological averaged monthly wind speeds at all stations, except at SETORS, where the wind speed ranged only from 0.79 to 1.26 m/s. Generally, the wind speed was relatively lower during the monsoon season than the non-monsoon periods, particularly at QOMS, BJ, NAMORS and MAWORS, where wind speeds in winter were the highest throughout the year, while the largest values of wind speed were observed in spring at NADORS.

3.1.2 Air temperature

Air temperature is available at different heights at NAMORS (1.5, 2.0, 4.0, 10 and 20 m), QOMS (1.5, 2.0, 4.0, 10 and 20 m), SETORS (1.3, 4.94, 9.95 and 18 m) and MAWORS (1.9 m). Air temperatures were recorded at one single height of 1.5m at NDORS and two heights of 1.03 and 8.41 m at BJ during 2006 to 2014. Identical to the wind sensor configuration, an air temperature gradient observation system with temperature probes at four heights (1.5, 3.0, 6.0 and 12 m) was used at BJ since 2015.

The multi-year monthly averaged diurnal variations of air temperature (Figure 2d) show that the values at NAMORS, QOMS and MAWORS were below 0°C in November, December, January and February. At BJ, the air temperature in January was below 0°C and the maximum values in December and February were also around freezing (1.17°C and 0.72°C, respectively). As shown in Figure 2e, the minimum daily air temperatures at BJ, MAWORS, NAMORS and NADORS dropped below 0°C from mid-October until the end of March or early April of the following year, but they were approximately 5°C higher at QOMS and SETORS. These differences in the variations in daily mean air temperature among stations are clearly shown in Figure 2f. In summer (June, July and August), the average daily and monthly air temperature at the lowest level at NADORS was the highest among the six stations. Moreover, wide variability was detected in the multi-year daily mean air temperatures at SETORS, especially in late March to early April, late May, and early December (Figure 2e). This abnormal variation indicates an instrument failure in the air temperature observations at 1.3 m at SETORS. Although this issue has been detected, the air temperature data provided at present are in raw format without any post-processing applied. Consequently, careful inspection is crucial when air temperature observations are required. In subsequent work, strict data quality control will allow problematic data to be identified and quality flags will be provided for each observational element.

3.1.3 Humidity

The heights of the humidity sensors are the same as those of the air temperature probes. Besides the relative humidity, up to four layers of water vapor pressure observations are also available at MAWORS (1.9 m), NADORS (1.5 and 2.8 m) and BJ (only available for the period 2015-2016, at 1.5, 3, 6, and 12 m); the heights of the water vapor pressure sensors at BJ are consistent with the heights of air temperature during the period from 2015 to 2016. It should be noted that the unit of water vapor pressure is kPa at MAWORS and NADORS, while it is 0.1 hPa at BJ.

The relative humidity showed obvious diurnal variations, peaking in the afternoon (Figure 2g). Compared with the magnitude of diurnal variations in summer, the diurnal range of relative humidity at SETORS in winter and spring was much greater, reaching 50%, and the maximum value of the average diurnal cycle of relative humidity was about 80%, which is also significantly higher than those at other stations. In contrast, the diurnal variability during the monsoon season was much smaller than that at BJ, QOMS, NAMORS and MAWORS. The monthly relative humidity is lowest at NADORS, however, there was a marked increase in summer due to the transition of mid-latitude westerlies to the Asian summer monsoon. Differences in humidity among the six stations presented in the diurnal and daily relative humidity records are clearly reflected in the seasonal variations at the monthly scale.

3.1.4 Air pressure

Barometers produced by Vaisala were installed at each station. Compared with variations in wind speed, air temperature and relative humidity, the diurnal and seasonal variations in air pressure are not obvious (Figure 2j-l), and pressure remained at a relatively stable level throughout the year. Air pressure is elevation-dependent amongst the six stations, with the highest value at SETORS and the lowest value at NAMORS, while a consistent diurnal and seasonal variations were found both at QOMS and NADORS of similar altitude.

3.1.5 Precipitation

Precipitation is measured at all stations except for MAWORS, either with tipping buckets or weighting gauges. At BJ and NADORS, the cumulative precipitation is recorded, while the total half-hourly precipitation is recorded at NAMORS, QOMS and SETORS. For the cumulative precipitation, negative growth resulting from the evaporation from the rain gauge can seriously affect accuracy. Moreover, large errors can be introduced in the precipitation time series by wind-induced under-catch, wetting loss, evaporation loss, and underestimation of trace precipitation amounts; it is difficult to apply bias correction to account for these losses (Goodison et al., 1998). While precipitation data are extremely valuable, accurate measurement is notoriously difficult due to the large errors mentioned above, particularly in cold regions such as the TP. Therefore, in the released datasets, the precipitation data are provided in raw format without any post-processing, which might potentially be underestimated, thus further bias correction or data selection is necessary before the precipitation observations are used.

3.2 Surface radiations

Radiation observations are an important component of surface meteorological observations and are released as a separate category. A four-component radiation flux observing system was installed at each station. The surface radiation flux monitoring system consists of upward and downward pyranometers for outgoing and incoming shortwave radiation flux; and upward and downward pyranometers for outgoing and incoming long-wave radiation flux.

Figure 3a-c shows that the diurnal variations in downward shortwave radiation flux at QOMS are the highest among the six stations, and the largest amplitude occurred in April with a range of 0-1027W m^{-2}. In winter, the MAWARS showed the smallest diurnal variation in downward shortwave radiation flux, while the variations at SETORS were the smallest in other seasons. When combined with the relatively higher solar radiation flux in this area, variations in upward shortwave radiation flux at QOMS were relatively high (Figure 3d). The multi-year averaged daily series showed wide fluctuations in upward shortwave radiation at NAMORS in September and October, as well as at QOMS in the winter and spring (Figure 3e), which may result from high fractional snow cover during these periods. In the early of the summer monsoon, the downward shortwave radiation decreased gradually with increasing cloud cover, as a result of the increase of moisture in the upper atmosphere. Both the incoming and outgoing long-wave radiation flux at each station (Figure 3g-i and 3j-l, respectively) showed significant seasonal variations, with high values in summer and low values in winter because of its dependence on ground temperatures. Upward longwave radiation flux at QOMS was higher than that at other stations (excluding SETORS) except in July and August when NADORS showed the largest values (Figure 3k and 3l, note the time series of longwave radiation fluxes at SETORS are not plotted in Figure 3 because of monitoring problems, but some of the remaining valid observations show that the longwave radiation fluxes at SETORS are the largest among all the stations). These differences showed high consistency with the differences in uppermost layer soil temperature as shown in Figure 5d-f.

3.3 EC data

The EC technique was applied to provide high-quality and continuous surface turbulent flux data for momentum and sensible and latent heat. The EC system comprises a sonic anemometer (CSAT3, Campbell Scientific, Inc.) and a fast-response hygrometer (LI-7500 open-path gas analyzer, Li-COR). All of the turbulence data were processed and quality-controlled using the TK3 software package (Mauder and Foken, 2011); the main processing steps were as follows: excluding physically invalid values and spikes, revising the time delay of the high-frequency water vapor and carbon dioxide sampling, planar fit coordinate rotation, correction of the loss of frequency response, correction of the ultrasonic virtual temperature and density fluctuations. The quality of each turbulent flux data series was evaluated by using the stationarity test and integral turbulence characteristics test. By combining the quality flags for stationarity and the integral turbulence characteristics test, a final quality flag (1-9) was assigned to each specific turbulent flux value except those for BJ, where classes 0-2 were used. Classes 1-3 (or 0 at BJ) indicate good quality suitable for fundamental research purposes, and classes 4-6 (1 at BJ) indicate suitability for general use, such as long-term analysis. Classes 7-9 (2 at BJ) should be rejected. The multi-year diurnal variation and seasonal variation of sensible and latent heat flux were calculated based on the data with medium or higher quality.

3.3.1 Sensible heat flux

As can be seen from the diurnal variations of sensible heat flux shown in Figure 4a, the sensible heat fluxes at all stations were negative at night. During the period from March to October, the atmospheric heating effect on the ground at NADORS was the strongest during the night, while the magnitude of diurnal variation in the sensible heat flux was the lowest here among the six stations from April to September. The variations in sensible heat flux (Figure 4a-c) show that prior to the monsoon season, and the sensible heat flux was the main consumer of available surface energy, then the diurnal variation in sensible heat flux decreased significantly with the onset of summer monsoon and was comparable to the latent heat flux. In other words, sensible heat flux exchanges prevail during the pre-monsoon periods. The timing of the onset of decreasing sensible heat flux following the spring maximum varied, occurring earliest at SETORS and NAMORS, followed by BJ and NADORS. Influenced by the interactions between the midlatitude westerlies and the summer monsoon, the summer sensible heat fluxes were significantly lower than those in spring at all stations.

3.3.2 Latent heat flux

In contrast to the bimodal pattern of the seasonal variations in sensible heat flux, the seasonal variation in latent heat flux revealed a unimodal pattern, that is, the latent heat flux was small during the pre-monsoon period, and when monsoon outbreaks, it increased rapidly as precipitation became frequent and the surface soil turned wet. The latent heat flux then increased gradually and it became comparable to the sensible heat flux during the summer monsoon period. A comparison of the seasonal variation of sensible heat flux (Figure 4c) and latent heat flux (Figure 4f) reveals that the latent heat flux was more significant to the sensible heat flux during the Asia summer monsoon season. During this period, the latent heat flux predominated in the surface energy budget (excluding the QOMS and NADORS), and the magnitudes of diurnal variations of latent heat flux were greatest at SETORS and BJ, and weakest in the desert landscapes of QOMS and NADORS (Figure 4d).

3.3.3 Carbon dioxide flux

The carbon dioxide flux is an important component of the atmospheric carbon balance and is a very important variable in the study of global climate change. As one of the key components of the EC monitoring system, the observed carbon dioxide fluxes at each station are provided through the density correction and frequency response correction applied by the TK3 software package (Mauder and Foken, 2011). A previous study has reported that the self-heating of the infrared gas analyzer in the open-path EC system can cause notable differences in temperature between the observation path and the ambient air, which may result in signal distortion (Burba et al., 2008); therefore, it is necessary to apply a specific correction to the carbon dioxide flux data to eliminate the heating impact and to accurately reveal the intensity of carbon dioxide exchange in the TP ecosystem (Zhu et al., 2012). However, the heating effect of the instrument was not been considered in the carbon dioxide flux data provided in this manuscript. When these data are used in studies of carbon dioxide exchange or related works (for example, estimating the net ecosystem production and its components), this specific correction of the data is needed to fully account for the impact of instrumental heating on observations.

3.4 Soil hydrothermal observations

3.4.1 Ground temperature

Ground temperatures at NADORS, SETORS and BJ are provided in this dataset. The variations in ground temperature show the weakest diurnal variations at BJ and the strongest at SETORS, where the ground temperature during the night was highest among the six stations. On the daily scale, the daily mean ground temperature at BJ was lower than that at SETORS and NADORS throughout the year, although its amplitude of the diurnal cycles was larger than that at the other two stations owing to the lower night-time temperatures (Figure 5a). Daily mean and monthly ground temperatures at BJ dropped below 0 °C during all months from October to April.

3.4.2 Soil temperature and soil moisture

Soil temperature and soil moisture are key physical quantities characterizing the land surface conditions and play important roles in controlling the energy and material interactions between land and the overlying atmosphere. To capture the continuous, real-time soil thermal and soil moisture conditions on different ground surfaces of the TP, five layers of soil profile sensors (soil temperature probes and water content reflectometers) were installed at SETORS (4, 10, 20, 60 and 100 cm), MAWORS (10, 20, 40, 80 and 160 cm) and NADORS (0, 20, 50, 100 and 200 cm). At NAMORS and QOMS, soil temperature and soil moisture were observed at depths of 0, 10, 20, 40, 80 and 160 cm. At BJ, soil temperature and soil water content were measured at four depths (0, 4, 10, 20 and 40 cm) during 2006-2014, and then at six depths (5, 10, 20, 40, 80 and 160 cm) during 2015-2016.

Figure 5a-f and Figure 5g-i demonstrate the variations of soil temperature and soil moisture, respectively, in the uppermost layer of each station (i.e., the top layer after excluding observations at a depth of 0 cm). Specifically, these were at depths of 4 cm at SETORS and BJ, 10 cm at MAWORS, NAMORS and QOMS, and 20 cm at NADORS. Soil temperature in the shallow layers show obvious variation at the diurnal scale, and are highly consistent with the variations in air temperature. The soil water content quickly responded to precipitation with an obvious increase with the onset of summer monsoon, particularly at BJ. Wiring problems at SETORS caused erroneous soil temperature and soil water content readings in all layers, which seriously affected the reliability of the respective observations. Although the two variables from SETORS are available in this dataset, data quality control and correction are needed.

3.4.3 Soil heat flux

Soil heat flux was measured by soil heat flux plates buried at BJ (10 and 20 cm for 2006-2014, 5 and 10 cm for 2015-2016), QOMS (10 cm) and SETORS (4, 10, 20, 60 and 100 cm). All the available soil heat flux data at each depth are released through this data descriptor. Due to abnormal fluctuations of the top-layer soil heat flux at QOMS and SETORS at both the diurnal and daily scale, only the variations in top-layer soil heat flux at BJ site were presented in Figure 5. The soil heat flux at BJ showed that it was usually relatively small and had evident diurnal and seasonal variations.

4 Data availability

Raw data were converted from binary mode to ASCII mode, and then key variables were extracted and saved as comma-separated values (.csv format). The CSV format was chosen as it is probably the most widely supported structured data format in scientific applications. All datasets presented and described in this article have been released and are available for free download from the Science Data Bank (http://www.dx.doi.org/10.11922/sciencedb.00103, Ma et al., 2020) and the TPDC (https://data.tpdc.ac.cn/en/data/b9ab35b2-81fb-4330-925f-4d9860ac47c3/). Special compressed files were designated for each station with four categories: turbulent flux data (FLUX), gradient meteorological data (GRAD), soil hydrothermal data (SOIL) and radiation data (RADM). Meanwhile, the yearly data integrity of each variable was also provided, with a value of 100 representing the absence of missing data. The heat maps shown in the Supplement are used to provide the data integrity information. These maps are very useful as they provide an intuitive depiction of the availability of each variable, facilitating data selection when analyzing land-atmosphere interactions and the structure of the PBL, driving land surface models, or evaluating model results.

5 Summary

As in-situ observations are scarce yet invaluable in cold regions, the model parameterization schemes are generally developed and evaluated based on a small number of sites, of which very few are located in high mountainous regions. Current numerical models suffer from a poor representation of the cold region processes, particularly on the TP (Xia et al., 2014; Toure et al., 2016; Orsolini et al., 2019; Xie et al., 2019). Long-term, high-quality and high temporal resolution observational data in the Third Pole region are not only extremely scarce, but are also very important for a deeper understanding of the key land surface processes. In this paper, a suite of land-atmosphere interactions observations from the integrated observation network over the TP is presented. Compared with previously open-accessed daily meteorological observations over the TP, this dataset provides the most comprehensive and high-quality continuous in-situ observations, with the highest temporal resolution (hourly) to date. Therefore, this fine-resolution data product can help to promote comprehensive scientific understanding of the interactions among the multi-sphere coupled systems over the TP and even the globe; to quantify uncertainties in satellite and model products; to assess the biases and gaps existing between the model simulations and reality; and to facilitate the development and improvement of land surface process models in cold regions. We hope that the datasets presented in this paper will contribute to these research areas and that they will be widely used in model development and evaluation.

Author contributions. YMM, ZYH, ZPX and BBW led the writing of this article and endorse the responsibility of the experimental site and the instruments. YMM and ZPX drafted the manuscript and ZPX led the consolidation of the dataset, prepared the data in the standardized format described in this paper and wrote this manuscript together with all co-authors.

Competing interests. The authors declare that they have no conflict of interests.

Acknowledgments. We would like to thank all the scientists, engineers, and students who participated in the field observations, maintained the observation instruments, and processed the observations.

Financial support. This work was supported by the Second Tibetan Plateau Scientific Expedition and Research (STEP) program (2019QZKK0103), the Strategic Priority Research Program of Chinese Academy of Sciences (XDA20060101), the National Natural Science Foundation of China (91837208), the National Key Research and Development Program of China (2018YFC1505701) and the National Natural Science Foundation of China (41905012, 41835650, 41975009, 41875031, 91737205, 41675106).

References

[1] Burba, G. G., McDERMITT, D. K., Grelle, A., Anderson, D. J., and Xu, L.: Addressing the influence of instrument surface heat exchange on the measurements of CO2 flux from open-path gas analyzers, Global Change Biology, 14, 1854-1876, 2008.

[2] Chen, D., Xu, B., Yao, T., Guo, Z., Cui, P., Chen, F., Zhang, R., Zhang, X., Zhang, Y., Fan, J., Hou, Z., and Zhang, T.: Assessment of past, present and future environmental changes on the Tibetan Plateau, Chinese Science Bulletin, 60, 3025, https://doi.org/10.1360/N972014-01370, 2015.

[3] Chen, X., Su, Z., Ma, Y., Yang, K., Wen, J., and Zhang, Y.: An Improvement of Roughness Height Parameterization of the Surface Energy Balance System (SEBS) over the Tibetan Plateau, Journal of Applied Meteorology and Climatology, 52, 607-622, https://doi.org/10.1175/jamc-d-12-056.1, 2013.

[4] Chen, X., Škerlak, B., Rotach, M. W., Añel, J. A., Su, Z., Ma, Y., and Li, M.: Reasons for the Extremely High-Ranging Planetary Boundary Layer over the Western Tibetan Plateau in Winter, Journal of the Atmospheric Sciences, 73, 2021-2038, https://doi.org/10.1175/jas-d-15-0148.1, 2016.

[5] Cheng, G., and Jin, H.: Permafrost and groundwater on the Qinghai-Tibet Plateau and in northeast China, Hydrogeology Journal, 21, 5-23, https://doi.org/10.1007/s10040-012-0927-2, 2013.

[6] Ding, Y.: Effects of the Qinghai-Xizang (Tibetan) plateau on the circulation features over the plateau and its surrounding areas, Advances in Atmospheric Sciences, 9, 112-130, https://doi.org/10.1007/BF02656935, 1992.

[7] Duan, A. M., and Wu, G. X.: Role of the Tibetan Plateau thermal forcing in the summer climate patterns over subtropical Asia, Climate Dynamics, 24, 793-807, https://doi.org/10.1007/s00382-004-0488-8, 2005.

[8] Goodison, B. E., Louie, P. Y., and Yang, D.: WMO solid precipitation measurement intercomparison, World Meteorological Organization Geneva, Switzerland, 1998.

[9] Immerzeel, W. W., van Beek, L. P. H., and Bierkens, M. F. P.: Climate Change Will Affect the Asian Water Towers, Science, 328, 1382-1385, https://doi.org/10.1126/science.1183188, 2010.

[10] Kang, S., Xu, Y., You, Q., Flügel, W.-A., Pepin, N., and Yao, T.: Review of climate and cryospheric change in the Tibetan Plateau, Environmental Research Letters, 5, 015101, https://doi.org/10.1088/1748-9326/5/1/015101, 2010.

[11] Li, M., Ma, Y., and Zhong, L.: The Turbulence Characteristics of the Atmospheric Surface Layer on the North Slope of Mt. Everest Region in the Spring of 2005, Journal of the Meteorological Society of Japan. Ser. II, 90C, 185-193, https://doi.org/10.2151/jmsj.2012-C13, 2012.

[12] Li, W., Guo, W., Qiu, B., Xue, Y., Hsu, P.-C., and Wei, J.: Influence of Tibetan Plateau snow cover on East Asian atmospheric circulation at medium-range time scales, Nature Communications, 9, 4243, https://doi.org/10.1038/s41467-018-06762-5, 2018.

[13] Liu, Y., Hoskins, B., and Blackburn, M.: Impact of Tibetan Orography and Heating on the Summer Flow over Asia, Journal of the Meteorological Society of Japan. Ser. II, 85B, 1-19, https://doi.org/10.2151/jmsj.85B.1, 2007.

[14] Ma, Y., Yao, T., and Wang, J.: Experimental study of energy and water cycle in Tibetan plateau-The progress introduction on the study of GAME/Tibet and CAMP/Tibet, Plateau Meteorology, 25, 344-351, 2006.

[15] Ma, Y., Kang, S., Zhu, L., Xu, B., Tian, L., and Yao, T.: Tibetan observation and research platform: atmosphere–land interaction over a heterogeneous landscape, Bulletin of the American Meteorological Society, 89, 1487-1492, 2008.

[16] Ma, Y., Zhu, Z., Amatya, P. M., Chen, X., Hu, Z., Zhang, L., Li, M., and Ma, W.: Atmospheric boundary layer characteristics and land−atmosphere energy transfer in the Third Pole area, Proc. IAHS, 368, 27-32, https://doi.org/10.5194/piahs-368-27-2015, 2015.

[17] Ma, Y., Hu, Z., Xie Z., Ma W., Wang B., Chen X., Li M., Zhong L., Sun F., Gu L., Han C., Zhang L., Liu X., Ding Z., Sun G., Wang S., Wang Y., Wang Z.: A long-term (2005-2016) dataset of integrated land-atmosphere interaction observations on the Tibetan Plateau. V1, Science Data Bank, http://www.dx.doi.org/10.11922/sciencedb.00103, 2020.

[18] Manabe, S., and Broccoli, A. J.: Mountains and Arid Climates of Middle Latitudes, Science, 247, 192-195, https://doi.org/10.1126/science.247.4939.192, 1990.

[19] Mauder M and Foken T.: Documentation and instruction manual of the eddy covariance software package TK3, Work Report University of Bayreuth, Dept. of Micrometeorology, ISSN: 1614-8916, pp. 46, 58, 2011.

[20] Orsolini, Y., Wegmann, M., Dutra, E., Liu, B., Balsamo, G., Yang, K., de Rosnay, P., Zhu, C., Wang, W., Senan, R., and Arduini, G.: Evaluation of snow depth and snow cover over the Tibetan Plateau in global reanalyses using in situ and satellite remote sensing observations, The Cryosphere, 13, 2221-2239, https://doi.org/10.5194/tc-13-2221-2019, 2019.

[21] Pan, B., Li, J., and Chen, F.: Qinghai-Xizang Plateau-a driver and amplifier of the global climatic change J, Lanzhou University (Natural Science Edition), 32, 08-115, 1996.

[22] Pepin, N. C., and Lundquist, J. D.: Temperature trends at high elevations: Patterns across the globe, Geophysical Research Letters, 35, https://doi.org/10.1029/2008gl034026, 2008.

[23] Pitman, A. J.: The evolution of, and revolution in, land surface schemes designed for climate models, International Journal of Climatology, 23, 479-510, https://doi.org/10.1002/joc.893, 2003.

[24] Qiu, J, The Third Pole-Climate Changes coming fast and furious to the Tibetan Plateau, Nature,454(7203),393-396, 2008.

[25] Sellers, P. J., Dickinson, R. E., Randall, D. A., Betts, A. K., Hall, F. G., Berry, J. A., Collatz, G. J., Denning, A. S., Mooney, H. A., Nobre, C. A., Sato, N., Field, C. B., and Henderson-Sellers, A.: Modeling the Exchanges of Energy,

Water, and Carbon Between Continents and the Atmosphere, Science, 275, 502-509, https://doi.org/10.1126/science.275.5299.502, 1997.

[26] Sun, F., Ma, Y., Ma, W., and Li, M.: One observational study on atmospheric boundary layer structure in Mt. Qomolangma region, Plateau Meteorology, 25, 1014-1019, 2006.

[27] Tao, S., Luo, S., and Zhang, H.: The Qinghai-Xizang Plateau Meteorological Experiment (Qxpmex) May–August 1979, Proceedings of International Symposium on the Qinghai-Xizang Plateau and Mountain Meteorology, 1986, 3-13,

[28] The NCAR Command Language (Version 6.6.2) [Software]: Boulder, Colorado: UCAR/NCAR/CISL/TDD. http://dx.doi.org/10.5065/D6WD3XH5, 2019.

[29] Toure, A. M., Rodell, M., Yang, Z.-L., Beaudoing, H., Kim, E., Zhang, Y., and Kwon, Y.: Evaluation of the Snow Simulations from the Community Land Model, Version 4 (CLM4), Journal of Hydrometeorology, 17, 153-170, https://doi.org/10.1175/jhm-d-14-0165.1, 2016.

[30] Wang, B., Ma, Y., Ma, W., and Su, Z.: Physical controls on half-hourly, daily, and monthly turbulent flux and energy budget over a high-altitude small lake on the Tibetan Plateau, Journal of Geophysical Research: Atmospheres, 122, 2289-2303, https://doi.org/10.1002/2016jd026109, 2017.

[31] Wang, J.: Land surface process experiments and interaction study in China-From HEIFE to IMGRASS and GAME-TIBET/TIPEX, Plateau Meteorology, 18, 280-294, 1999.

[32] Wu, G., Zhuo, H., Wang, Z., and Liu, Y.: Two types of summertime heating over the Asian large-scale orography and excitation of potential-vorticity forcing I. Over Tibetan Plateau, Science China Earth Sciences, 59, 1996-2008, https://doi.org/10.1007/s11430-016-5328-2, 2016.

[33] Xia, K., Wang, B., Li, L., Shen, S., Huang, W., Xu, S., Dong, L., and Liu, L.: Evaluation of snow depth and snow cover fraction simulated by two versions of the flexible global ocean-atmosphere-land system model, Advances in Atmospheric Sciences, 31, 407-420, 10.1007/s00376-013-3026-y, 2014.

[34] Xiao, Z., and Duan, A.: Impacts of Tibetan Plateau Snow Cover on the Interannual Variability of the East Asian Summer Monsoon, Journal of Climate, 29, 8495-8514, https://doi.org/10.1175/jcli-d-16-0029.1, 2016.

[35] Xie, Z., Hu, Z., Xie, Z., Jia, B., Sun, G., Du, Y., and Song, H.: Impact of the snow cover scheme on snow distribution and energy budget modeling over the Tibetan Plateau, Theoretical and Applied Climatology, 131, 951-965, https://doi.org/10.1007/s00704-016-2020-6, 2018.

[36] Xie, Z., Hu, Z., Ma, Y., Sun, G., Gu, L., Liu, S., Wang, Y., Zheng, H., and Ma, W.: Modeling Blowing Snow Over the Tibetan Plateau With the Community Land Model: Method and Preliminary Evaluation, Journal of Geophysical Research: Atmospheres, 124, 9332-9355, https://doi.org/10.1029/2019jd030684, 2019.

[37] Yanai, M., Li, C., and Song, Z.: Seasonal Heating of the Tibetan Plateau and Its Effects on the Evolution of the Asian Summer Monsoon, Journal of the Meteorological Society of Japan. Ser. II, 70, 319-351, https://doi.org/10.2151/jmsj1965.70.1B_319, 1992.

[38] Yang, K., Koike, T., and Yang, D.: Surface Flux Parameterization in the Tibetan Plateau, Boundary-Layer Meteorology, 106, 245-262, https://doi.org/10.1023/A:1021152407334, 2003.

[39] Yang, K., Koike, T., Fujii, H., Tamura, T., Xu, X., Bian, L., and Zhou, M.: The daytime evolution of the atmospheric boundary layer and convection over the Tibetan Plateau: observations and simulations, Journal of the Meteorological Society of Japan. Ser. II, 82, 1777-1792, 2004.

[40] Yang, K., Chen, Y.-Y., and Qin, J.: Some practical notes on the land surface modeling in the Tibetan Plateau, Hydrology and Earth System Sciences, 13, 687-701, 2009.

[41] Yao, T., Thompson, L., Yang, W., Yu, W., Gao, Y., Guo, X., Yang, X., Duan, K., Zhao, H., Xu, B., Pu, J., Lu, A., Xiang, Y., Kattel, D. B., and Joswiak, D.: Different glacier status with atmospheric circulations in Tibetan Plateau and surroundings, Nature Climate Change, 2, 663-667, https://doi.org/10.1038/nclimate1580, 2012.

[42] Ye, D., and Wu, G.: The role of the heat source of the Tibetan Plateau in the general circulation, Meteorology and Atmospheric Physics, 67, 181-198, https://doi.org/10.1007/BF01277509, 1998.

[43] Zhong, L., Zou, M., Ma, Y., Huang, Z., Xu, K., Wang, X., Ge, N., and Cheng, M.: Estimation of Downwelling Shortwave and Longwave Radiation in the Tibetan Plateau Under All-Sky Conditions, Journal of Geophysical Research: Atmospheres, 124, 11086-11102, https://doi.org/10.1029/2019jd030763, 2019.

[44] Zhou, Y., and Guo, D.: Principal characteristics of permafrost in China, Journal of Glaciology and Geocryology, 1, 1982.

[45] Zhu, X., Yu, G., Wang, Q., ZHANG, M., HAN, S., ZHAO, X., and YAN, J.: Instrument heating correction effect on estimation of ecosystem carbon and water fluxes, Chinese Journal of Ecology, 31, 487-493, 2012.

Table 1. List of the geographic characteristics of the six sites.

Site	Latitude	Longitude	Elevation (m)	Land cover	Soil type
BJ	31.37°N	91.90°E	4509	Alpine meadow	Sandy silt loam
QOMS	28.36°N	86.95°E	4298	Alpine desert	Sand and gravel
SETORS	29.77°N	94.74°E	3327	Alpine meadow	Sandy clay loam
NADORS	33.39°N	79.70°E	4270	Alpine desert	Sand and gravel
MAWORS	38.42°N	75.03°E	3668	Alpine desert	Sand and gravel
NAMORS	30.77°N	90.96°E	4730	Alpine steppe	Sandy silt loam

https://doi.org/10.5194/essd-2020-85
Preprint. Discussion started: 17 July 2020

Table 2. Overview of the sensors used at each station.

Site	Variables	Sensors models	Manufacturers	Period	Heights	Units
BJ	Air temperature	HMP45D HMP155	Vaisala Vaisala	2006-2014 2015-2016	1.03 and 8.41m 1.5, 3, 6, and 12m	ºC
	Wind speed and direction	05103 WindSonic	RM Young Gill	2006-2014 2015-2016	0.91, 5.02, and 10.36m 1.5, 3, 6, and 12m	m/s and degree
	Humidity	HMP45D HMP155	Vaisala Vaisala	2006-2014 2015-2016	1.03 and 8.41m 1.5, 3, 6, and 12m	%
	Pressure	PTB220C	Vaisala	2006-2014	-	hPa
	Radiations	CM21 for shortwave radiation PIR for longwave radiation	Kipp & Zonen Eppley	2006-2016	-	W m^{-2}
	Precipitation	NOAH-II T200B	ETI Geonor	2006-2014 2015-2016	-	mm
	Soil temperature	TS-301 TR-219L	Okazaki Tri-Tronics	2006-2014 2015-2016	0.04, 0.1, 0.2, and 0.4m 0.05, 0,1, 0.2, 0.4, 0.8 and 1.6m	ºC
	Soil moisture	CS616-L CS616-L	Campbell Campbell	2006-2014 2015-2016	0.04 and 0.2m 0.05, 0,1, 0.2, 0.4, 0.8 and 1.6m	v/v %
	Soil heat flux	HFP01 HFP01	Hukseflux Hukseflux	2006-2014 2015-2016	0.1and 0.2 m 0.05 and 0.1m	W m^{-2}
	EC	CSAT3 LI-7500	Campbell Li-COR	2006-2016	3.02m	
QOMS	Air temperature	HMP45C-GM	Vaisala	2005-2016	1.5, 2, 4, 10, and 20m	ºC
	Wind speed and direction	034B	MetOne	2005-2016	1.5, 2, 4, 10, and 20m	m/s and degree
	Humidity	HMP45C-GM	Vaisala	2005-2016	1.5, 2, 4, 10, and 20m	%
	Pressure	PTB220A	Vaisala	2005-2016	-	hPa
	Radiations	CNR1	Kipp & Zonen	2005-2016	-	W m^{-2}
	Precipitation	RG13H	Vaisala	2005-2016	-	mm
	Soil temperature	Model 107	Campbell	2005-2016	0, 0.1, 0.2, 0.4, 0.8 and 1.6m	ºC
	Soil moisture	CS616	Campbell	2005-2016	0, 0.1, 0.2, 0.4, 0.8 and 1.6m	v/v %
	Soil heat flux	HFP01	Hukseflux	2005-2016	0.05m	W m^{-2}
	EC	CSAT3 LI-7500	Campbell Li-COR	2007-2016	3.25m	
SETORS	Air temperature	HMP45C-GM	Vaisala	2007-2016	1.3, 4.94, 9.95, and 18m	ºC
	Wind speed and direction	034B	MetOne	2007-2016	1.3, 4.94, 9.95, and 18m	m/s and degree
	Humidity	HMP45C-GM	Vaisala	2007-2016	1.3, 4.94, 9.95, and 18m	%
	Pressure	PTB220A	Vaisala	2007-2016	-	hPa
	Radiations	CNR1	Kipp & Zonen	2007-2016	-	W m^{-2}

	Precipitation	RG13H	Vaisala	2007-2016	-	mm
	Soil temperature	Model 107	Campbell	2007-2016	0.04, 0.1, 0.2, 0.6 and 1m	ºC
	Soil moisture	CS616	Campbell	2007-2016	0.04, 0.1, 0.2, 0.6 and 1m	v/v
	Soil heat flux	HFP01	Hukseflux	2007-2016	0.04, 0.1, 0.2, 0.6 and 1m	W m^{-2}
	EC	CSAT3 LI-7500	Campbell Li-COR	2007-2016	3.04m	m s^{-1}
NADORS	Air temperature	HMP45C	Vaisala	2009-2016	1.5m	ºC
	Wind speed and direction	05013	RM Young	2009-2016	1.5m	m/s and degree
	Relative humidity	HMP45C	Campbell	2009-2016	1.5 and 2.8m	%
	Water vapor pressure	HMP45C	Campbell	2009-2016	1.5 and 2.8m	kPa
	Pressure	PTB210	Vaisala	2009-2016	-	hPa
	Radiations	NR01	Kipp & Zonen	2009-2016	-	W m^{-2}
	Precipitation	T-200B	Geonor	2009-2016	-	mm
	Soil temperature	CSI 109	Campbell	2011-2016	0, 0.2, 0.5, 1.0 and 2.0m	ºC
	Soil moisture	CS616	Campbell	2011-2016	0, 0.2, 0.5, 1.0 and 2.0m	v/v
	EC	CSAT3 and LI-7500	Campbell and Li-COR	2005-2016	2.75m	
MAWORS	Air temperature	HMP155A	Vaisala	2010-2016	1.9m	ºC
	Wind speed and direction	05103-L	RM Young	2010-2016	2m	m/s and degree
	Relative humidity	HMP155A	Vaisala	2010-2016	1.9m	%
	Water vapor pressure	HMP155A	Vaisala	2010-2016	1.9m	kPa
	Pressure	PTB210	Vaisala	2010-2016	-	hPa
	Radiations	NR01	Kipp & Zonen	2010-2016	-	W m^{-2}
	Soil temperature	CSI 109	Campbell	2010-2016	0.1, 0.2, 0.4, 0.8 and 1.60m	ºC
	Soil moisture	CS616	Campbell	2010-2016	0.1, 0.2, 0.4, 0.8 and 1.60m	v/v
	EC	CSAT3 LI-7500	Campbell Li-COR	2010-2016	2.3m	
NAMORS	Air temperature	HMP45D	Vaisala	2005-2016	1.5, 2.0, 4.0, 10.0 and 20.0m	ºC
	Wind speed and direction	WAA151	Vaisala	2005-2016	1.5, 2.0, 4.0, 10.0 and 20.0m	m/s and degree
	Humidity	HMP45D	Vaisala	2005-2016	1.5, 2.0, 4.0, 10.0 and 20.0m	%
	Pressure	PTB210	Vaisala	2005-2016	-	hPa
	Radiations	CMP6	Vaisala	2005-2016	-	W m^{-2}
	Precipitation	RG13H	Vaisala	2005-2016	-	mm
	Soil temperature	Model 107	Campbell	2005-2016	0, 0.1, 0.2, 0.4, 0.8, 1.6m	ºC
	Soil moisture	CS616	Campbell	2005-2016	0, 0.1, 0.2, 0.4, 0.8, 1.6m	v/v %
	EC	CSAT3 LI-7500	Campbell Li-COR	2005-2016	3.06m	

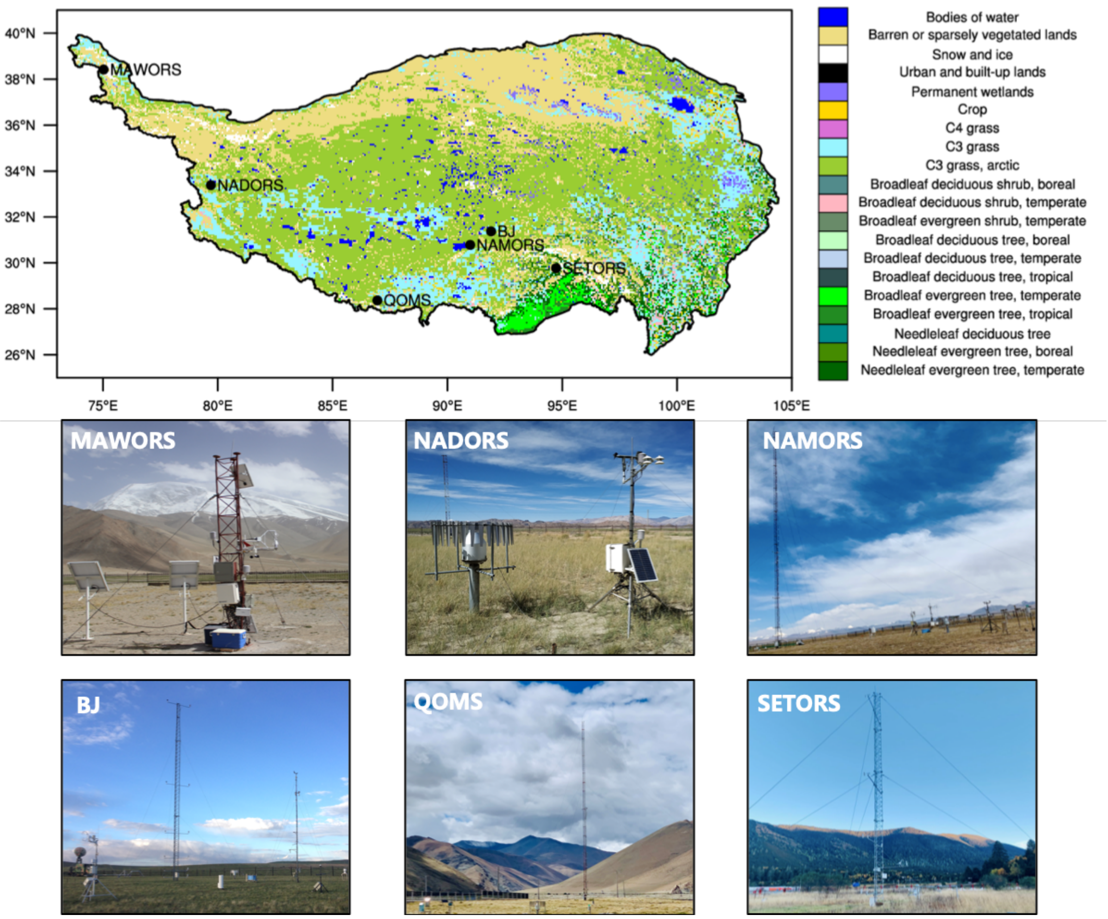

Figure 1. The integrated land-atmosphere observation network on the TP. At each site, the near surface atmospheric conditions are sampled with multilayer wind speed and direction, air temperature and humidity instruments. Surface pressure, precipitation and four-component surface radiation fluxes are also measured. Vertical profiles of soil temperature and soil moisture content are monitored by multilayer temperature probes and water content reflectometers. An open path eddy covariance turbulent measurement system is installed at each site to provide continuous monitoring of the vertical turbulent fluxes within the atmospheric boundary layers [Colour figure can be viewed in the online issue].

https://doi.org/10.5194/essd-2020-85
Preprint. Discussion started: 17 July 2020

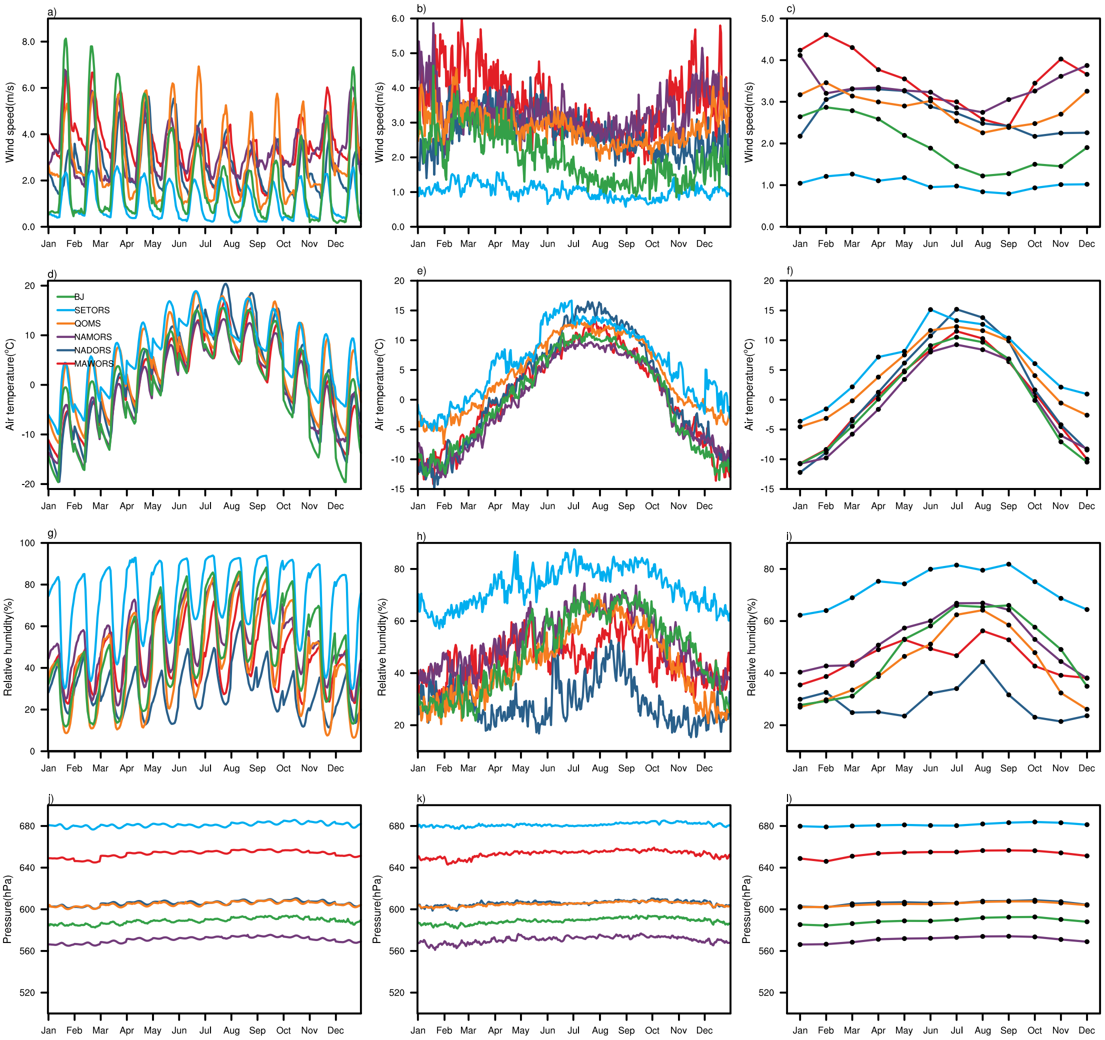

Figure 2. The climatological averages of the lowest-level of wind speed, air temperature, relative humidity and surface pressure at diurnal (left-most), daily (middle) and monthly (right-most) scales. For sites except BJ, the climatological mean of each variable was calculated based on all the available observations; for BJ, only the observations during the period of 2006-2014 were used [Colour figure can be viewed in the online issue].

https://doi.org/10.5194/essd-2020-85
Preprint. Discussion started: 17 July 2020

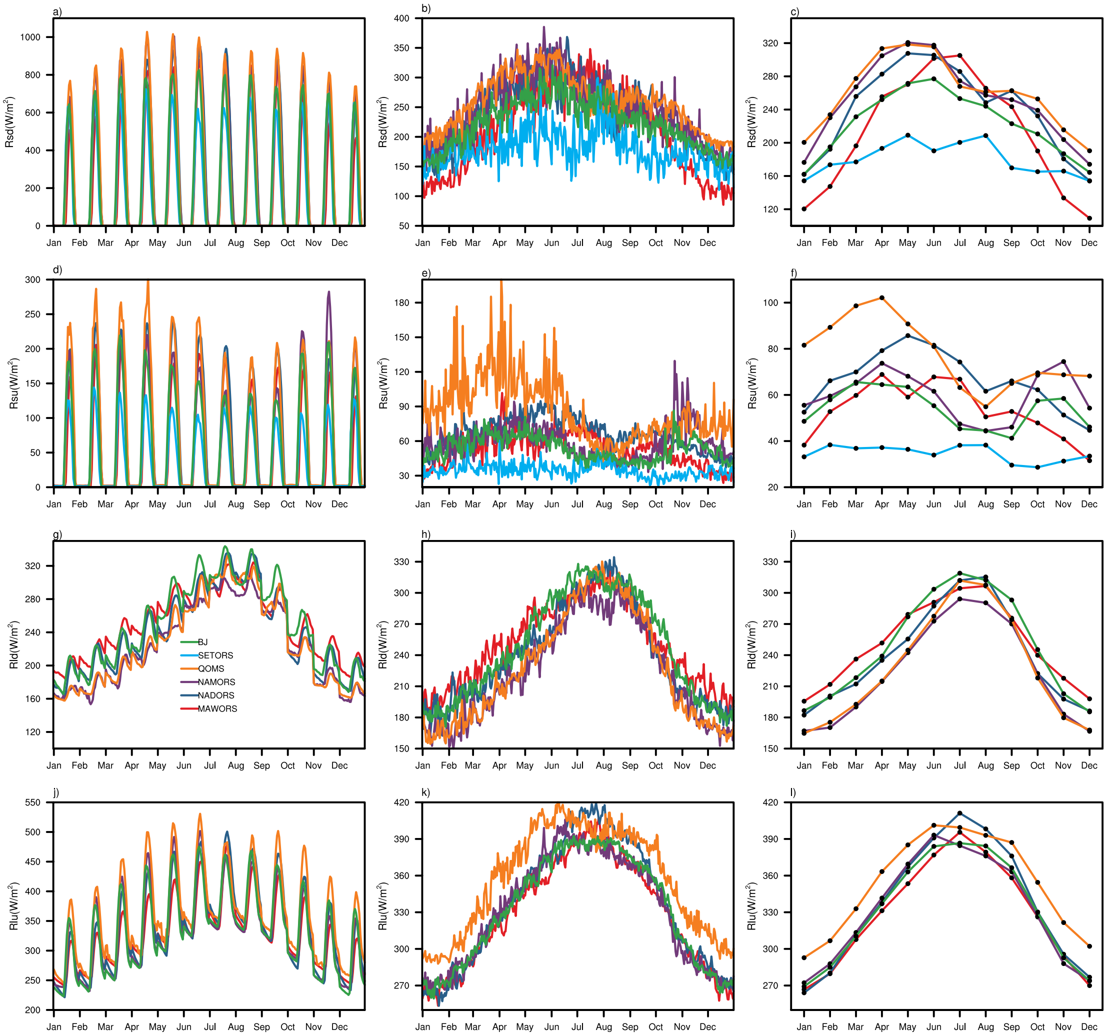

Figure 3. Same as Figure 2, but for the climatological average of the downward and upward solar radiation (Rsd and Rsu), and incoming and outgoing longwave radiation (Rld and Rlu), respectively [Colour figure can be viewed in the online issue].

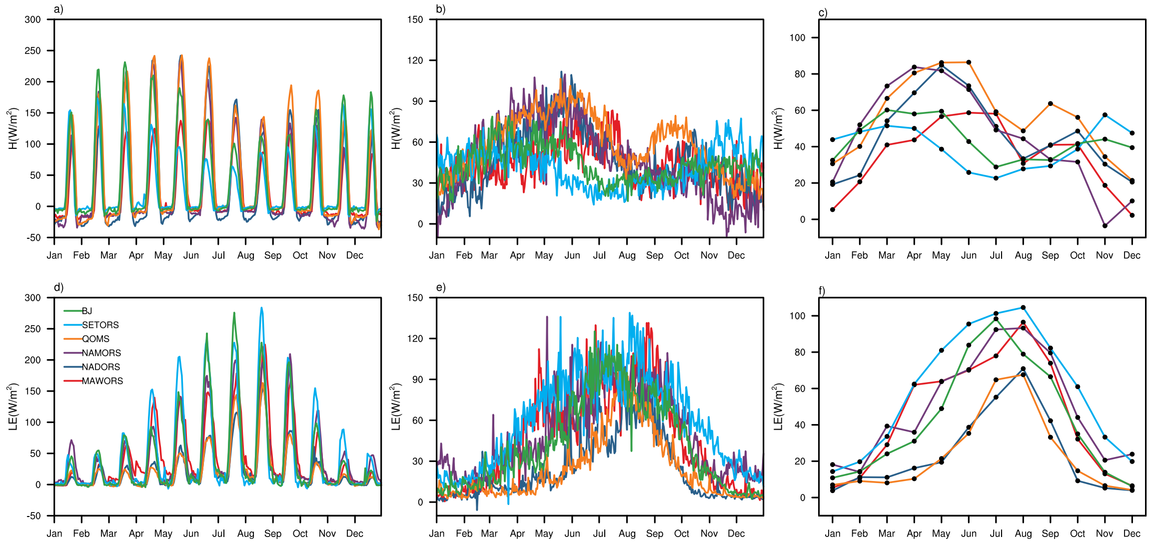

Figure 4. Same as Figure 2, but for the climatological average of the sensible heat flux (H) and latent heat flux (LE) variation, respectively [Colour figure can be viewed in the online issue].

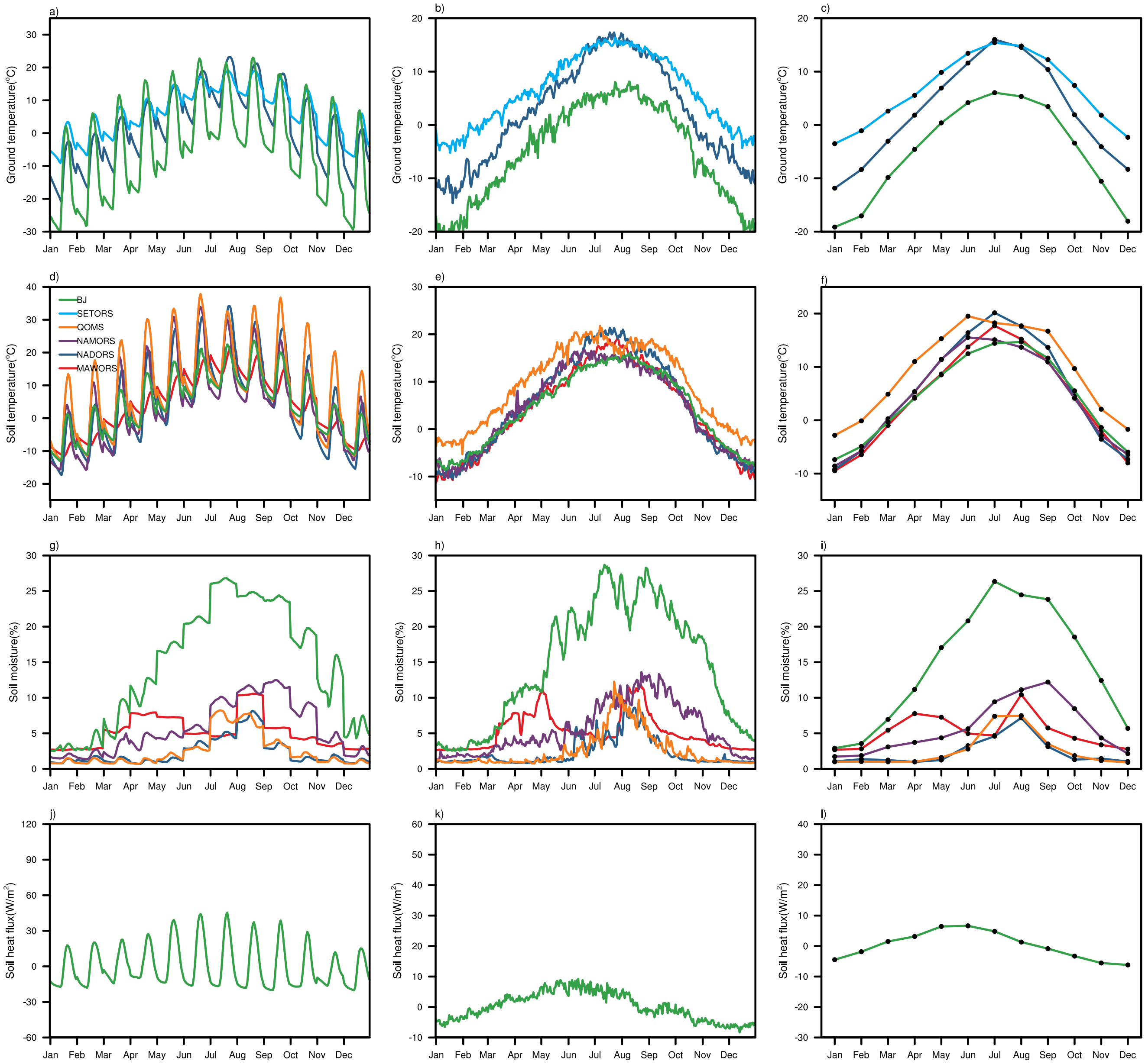

Figure 5. Same as Figure 2, but for the climatological average of ground temperature and first layer (except for the observations at depths of 0cm) soil temperature, soil moisture and soil heat flux, respectively [Colour figure can be viewed in the online issue].